Transient Flow-Induced Crystallization of a Polyethylene Melt

A. C. BUSHMAN,* A. J. MCHUGH

Department of Chemical Engineering, University of Illinois, Urbana, Illinois 61801

Received 25 April 1996; accepted 2 November 1996

ABSTRACT: Extensional, flow-induced crystallization (FIC) of a high-density polyethylene (HDPE) melt has been studied using a four-roll mill flow cell. Simultaneous measurement of the birefringence and scattering dichroism are used to quantify the crystallization process during and following transient flow deformation in planar extensional flow. Suspension of the HDPE phase as a droplet in a linear low-density polyethylene carrier phase prevents die blockage on crystallization and allows measurement of the flow kinematics. Initial crystallization rates following a transient flow deformation show a stress–strain dependence. Crystallization induction times during flow correlate with the extension rate during the transient flow deformation. Measurement of the HDPE melt steady and oscillatory flow rheological properties, along with measurements of time constants following step-shear and extensional strains, allow determination of the viscoelastic properties which enhance FIC. Parameters obtained from these experiments are used in a phenomenological model for FIC which allows qualitative and semiquantitative analysis of the data trends, particularly the relaxation behavior of the birefringence during flow cessation/crystallization. © 1997 John Wiley & Sons, Inc. J Appl Polym Sci **64:** 2165–2176, 1997

Key words: flow; crystallization; birefringence; dichroism; stress

INTRODUCTION

Flow-induced crystallization (FIC) occurs in virtually every process of industrial importance involving orientation of a crystallizable polymer melt. In confined-flow geometries, such as die extrusion and injection molding, orientation and crystallization take place under inherently transient conditions. In these cases, competition between flow and relaxation in the molten and semicrystalline states strongly influences the transformation kinetics and, ultimately, the properties of the crystallized product. While measurements of the crystallization kinetics in steady shear flows have been relatively common, measurements of crystallization in transient flows—particularly those involving extensional kinematics—have been relatively rare. In a recent article,[1] we presented a technique for direct observation of the flow, relaxation, and crystallization dynamics during transient, planar extensional flow of a high-density polyethylene (HDPE) melt. Uncontrolled crystallization and die blockage are avoided by suspending the HDPE phase as a droplet within a carrier phase of linear low-density polyethylene (LLDPE) which remains molten at the temperature of interest. Analyses of the droplet flow kinematics and crystallization kinetics were based on birefringence measurements, combined with *in situ* video imaging of the flow field. Although birefringence retardation is related to optical anisotropies induced by oriented crystallization, it also depends on the amorphous phase

Correspondence to: A. J. McHugh.

* *Present address:* International Paper Company, Loveland, OH 45140.

Contract grant sponsor: National Science Foundation; contract grant number: DMR 89-20538.

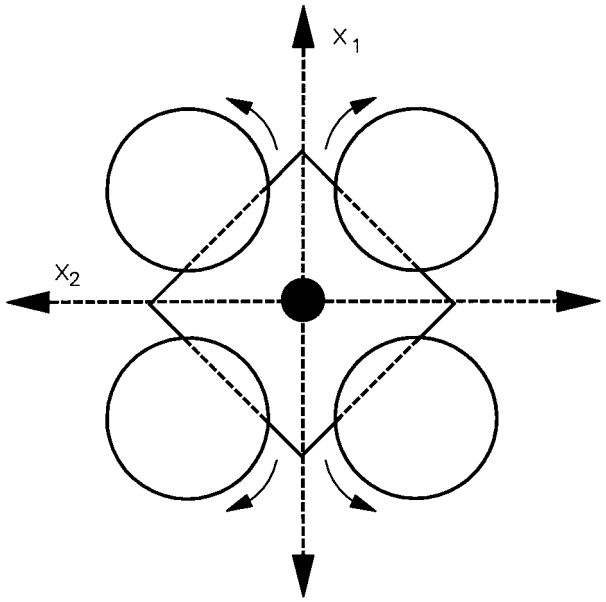

Figure 1 Schematic of four-roll mill flow cell illustrating coordinate system, directions of roller rotation, and initial placement of high density droplet (dark circle). Dotted square delineates optical window placement.

orientation which cannot be separated from the total signal during flow. Hence, quantitative analysis of the oriented crystallization was limited to the period following flow cessation.

The objective of this article is to present new results obtained in the same extensional flow geometry using a modified polarimetry setup allowing simultaneous measurement of the scattering dichroism and linear birefringence. The improved optics leads to a more direct analysis of the crystallization and relaxation dynamics following flow cessation, and allows determination of the crystallization induction time during flow. Rheological data have also been obtained on the droplet phase material. These data enable a more quantitative analysis of the viscoelastic properties that facilitate FIC. Moreover, data trends obtained in this and our previous study are compared with quantitative predictions obtained using a continuum-based model for FIC which we recently developed.[2]

EXPERIMENTAL

Flow Cell and Optics

Details of the four-roll mill device are given in the previous article.[1] Figure 1 shows a schematic of the flow cell, droplet placement, and coordinate system. The entire device is mounted to an extruder to allow filling with the molten carrier phase. Die wall temperature is monitored with a thermocouple and controlled (± 0.5°C) using a multichannel feedback system. Conversion to melt temperatures is achieved using a calibration based on thermocouple measurements made at the flow stagnation point. The precision of all reported melt temperatures is ± 0.5°C.

Two types of flow experiments are used. In the first, the suspended droplet is deformed for a short period (on the order of 1 min), followed by cessation of the flow, during which simultaneous relaxation and crystallization occur. In each run, video images arising from the birefringence and total scattering dichroism intensities are separately recorded. In the second case, droplet flow is continuous and images associated with the absorbance and retardation of the scattering dichroism are separately recorded. Figure 2 illustrates the general optical configuration. Digitizing software is used to convert the recorded image intensities and droplet shapes to quantitative data. Details of the optical alignment procedures and data analysis methods are given in ref. 3. For flow cessation runs, the polarizer along path B is removed and the first and second polarizers along optical path A are oriented at 45° and 135°, respectively. In this configuration, optical path A gives the birefringence intensity and path B gives the total intensity due to scattering dichroism. The fast axis of the crystallized droplet orients at 90° relative to the principal flow axis, indicating c-axis orientation of the crystallites. The sign of the dichroism is also positive, indicating that the direction of preferred crystal scattering is along the x_1-axis. The c-axis orientation of the crystallites has been confirmed by analysis of samples extracted from the flow device.[1] Since the optical and flow axes coincide, and the birefringence and dichroism are coaxial,[1] the transmittance, T, for any point in the image recorded by camera A will be given by

$$T = \frac{I}{I_o} = \frac{e^{-A_e}}{4}(\cosh \kappa - \cos \delta_T) \qquad (1)$$

where I_o and I are the incident and transmitted light intensities, respectively; κ is the phase shift of the dichroism; A_e is the turbidity (or absorbance) due to scattering; and δ_T is the total retardation of the birefringence along the optical path through the flow cell. Since the latter includes the droplet and carrier phases,

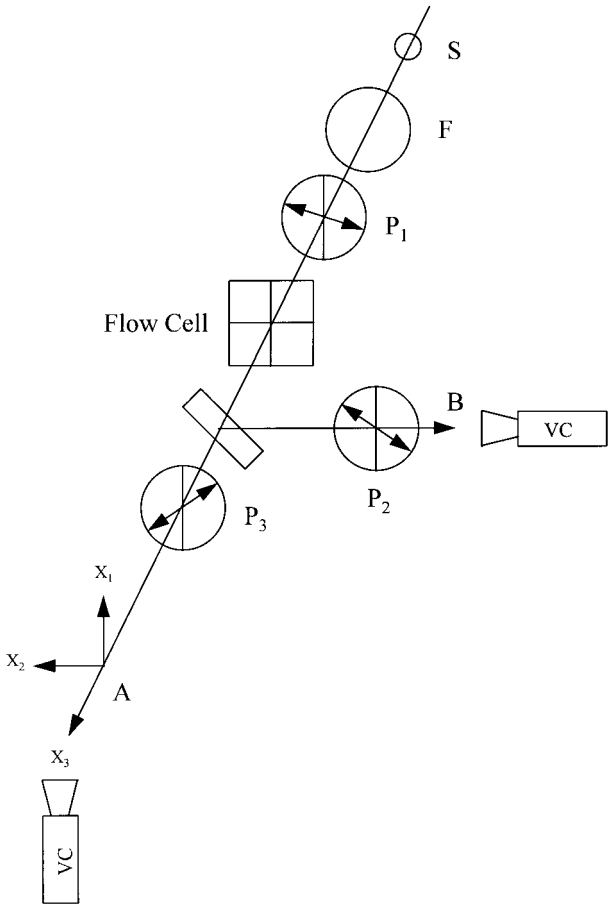

Figure 2 General polariscope configuration for image recording. Optical elements comprise a light source (S), filter (F), beam splitter, and polarizers (P_i). Polarizer transmission axes are rotated counterclockwise relative to the x_1 axis. For birefringence and dichroism intensity imaging, P_2 is removed and P_1 and P_3 are oriented at 45° and 135°, respectively. For simultaneous dichroism retardation and absorbance analysis, P_1 is removed and P_2 and P_3 are oriented at 90° and 0°, respectively.

$$\delta_T = \delta_a + \delta_{da} + \delta_c \tag{2}$$

Subscripts denote the amorphous carrier phase (a), the amorphous portion of the droplet phase (da), and the crystalline portion of the droplet phase (c). Images recorded by the camera along path B contain the dichroism retardation and turbidity given by

$$T = \frac{e^{-A_e}}{2} \cosh \kappa \tag{3}$$

The cosh κ term in eq. (3) remains close to unity during the initial period of crystallization.[1,3] Thus, assuming the amorphous relaxation at any point in the droplet can be described by a single time constant λ, the time dependence of the droplet crystalline birefringence will be given by

$$\delta_c = 2 \sin\left(\left(\frac{I_A I_{B_o}}{I_{A_o} I_B}\right)^{1/2}\right) - \delta_{da,o} e^{-t/\lambda} \tag{4}$$

The image intensities in eq. (4) are those recorded by either camera A or B in Figure 2.

For the continuous flow experiments, the first polarizer along path A is removed, the second polarizer is oriented at 0°, and the polarizer along path B is oriented at 90°. Thus the transmittance for either path A or B will be given by

$$T = \frac{e^{-A_e}}{2} [\cosh \kappa - \sinh \kappa \cos 2\alpha] \tag{5}$$

where α is 0° or 90°. Both κ and A_e are evaluated from the following equations:

$$\kappa = \frac{1}{2} \ln\left(\frac{I_B}{I_A}\right) \tag{6}$$

$$A_e = -\frac{1}{2} \ln\left(\frac{4 I_A I_B}{I_{A_o} I_{B_o}}\right) \tag{7}$$

Materials and Procedures

Droplet Phases

High-density polyethylene was used as the droplet phase and an LLDPE (melting point T_m = 122°C; Union Carbide, Port Lavaca, TX) was used for the carrier phase. The high-density phase was obtained by extruding a mixture of two high-molecular-weight polyethylenes (HMWPE; Celanese, Summit, NJ), designated A60-500 and F60-600, at 150°C using an Arbor press. Cylindrical pellets of the desired thickness (1.5–2.0 mm) and diameter ($\sim$ 2–3 mm) were cut from uniform lengths of the extrudate. In the results to be described, a 10 wt % A60-500/90% F60-600 mixture was used because it produced molten droplets which deformed uniformly and symmetrically in the carrier phase flow. The equilibrium melting point of the blend, determined by scanning calorimetry, is 142°C. Based on known molecular weight distributions of the two polymers, $\bar{M}_w$ and $\bar{M}_n$ of the blend were calculated to be 1.48×10^5 and 2.6×10^4, respectively. The quiescent crystallization kinetics of this system were studied in

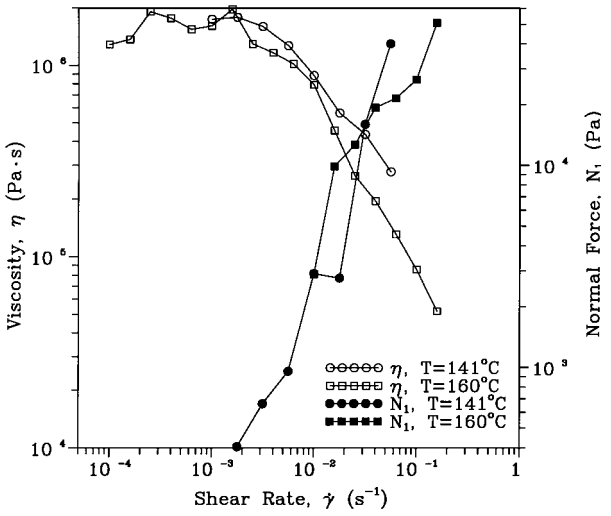

Figure 3 Steady-state shear viscosity and first normal stress difference behavior of the HDPE droplet phase material at 141°C and 160°C.

some detail,[4] and portions of these results were given in the previous article.[1] Transformation half-times were found to be several orders of magnitude greater than those under flow, suggesting that flow significantly affects the transformation kinetics, despite the relatively small deformation rates used in our experiments ($\sim 0.03\ s^{-1}$).

Further details of the experimental procedures, data analysis, and examples of video images of the droplet deformation/crystallization dynamics are given in ref. 3 and the previously mentioned article.[1]

Rheological Measurements

The relative magnitudes of the viscous and elastic responses of a polymer melt control its orientability and therefore its propensity to undergo FIC. To further evaluate this, steady-state shear viscosity–normal stress, and oscillatory flow, storage, and loss moduli were obtained for the droplet phase material using Rheometrics System Four and Weissenberg Rheogoniometers in the cone and plate geometry. A polydimethylsiloxane viscosity standard was also analyzed on both devices, and, in all cases, good agreement was found between the two instruments over a broad range of shear rates and oscillatory frequencies.[3] Because the droplet phase relaxation time plays an important role in the FIC, an evaluation of the melt relaxation behavior was also carried out using three different techniques: measurement of the droplet birefringence decay following flow cessation in the four-roll mill, analysis of the time-dependent relaxation modulus following a shear deformation in the rheometer, and fitting of the storage and loss moduli in oscillatory flow. Since fits of the oscillatory flow data required several relaxation times,[3] the discussion will be limited to results from the first two experiments in which a single time constant was found to be adequate. In all cases, the rheological experiments were carried out at temperatures above those at which crystallization would occur.

RESULTS

Rheological Properties

The steady-state viscometric properties of the 10% A60-500/90% F60-600 HMWPE droplet phase material at 141 and 160°C are shown in Figure 3. A decrease in viscosity with increased temperature and an increase in first normal stress difference with shear rate are the expected trends. The dynamic properties shown in Figure 4 were measured at 136°C, close to the temperatures used in the four-roll mill experiments but high enough to avoid shear-induced crystallization. The Cox-Merz rule leads to $|\eta^*|$ values slightly lower than those measured for the viscosity at higher temperatures. At the lowest frequen-

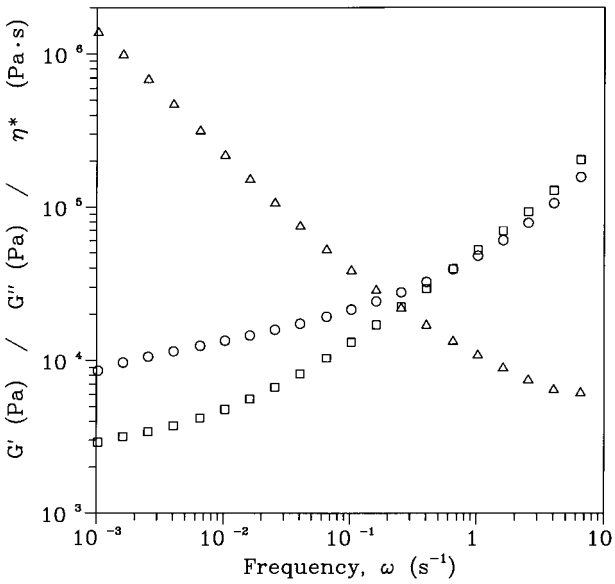

Figure 4 Frequency dependence of the oscillatory flow storage (G', ○), loss moduli (G'', □), and complex viscosity (η^*, △) of the HDPE droplet phase material at 136°C.

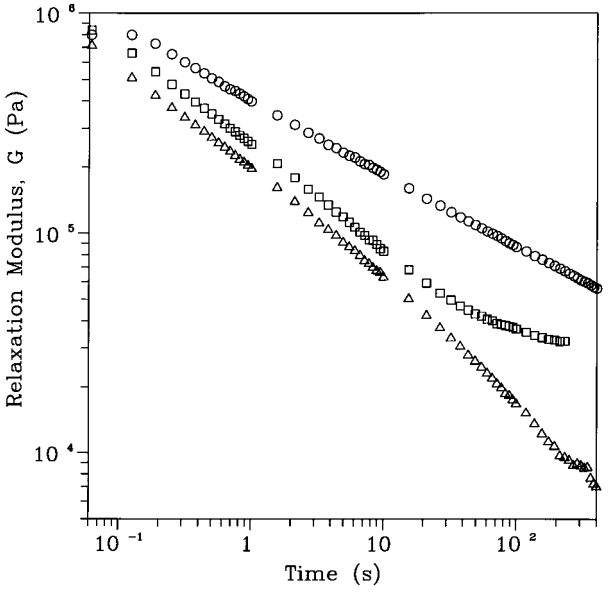

Figure 5 Time-dependent relaxation modulus (G) of the HDPE droplet phase material following a 60% step-shear strain at 141°C (○), 160°C (□), and 200°C (△).

cies, the storage and loss moduli, $G'(\omega)$ and $G''(\omega)$, respectively, exhibit a plateau behavior. Since $G'(\omega)$ is greater than $G''(\omega)$, the elastic nature of the material apparently dominates the viscoelastic response, even at extremely low frequencies. This behavior suggests that entanglements due to the high-molecular-weight species play a controlling role.

Figure 5 shows the relaxational responses following a 60% step-shear strain, for various temperatures ranging from 141 to 200°C. The relaxation modulus decreases with increased temperature, as expected. At each temperature, five different step-shear-strain experiments were run at strains ranging from 20 to 100%. The resulting curves showed strain hardening, perhaps attributable to a nonlinear material response. Wagner and Demarmels[5] have introduced a model which utilizes the concepts of "chain diffusion" governing the spectrum of relaxation times, independent of deformation, and, "loss of topological constraints" determining the nonlinear material response. It is likely that the high molecular weight fraction of the HMWPE causes entanglements which prevent relaxation as the applied strain is increased. We believe these entanglements control the orientability of the material and its crystallization under flow.

Figure 6 shows data for the droplet phase birefringence measured near the stagnation point in the four-roll mill, following flow cessation at the temperatures indicated. The first 10 s of the signal were discarded in order to remove all traces due to the faster-relaxing background carrier phase. The relaxation times indicated on the graphs were obtained by fitting the data to the following expression:

$$\delta_{da} = \delta_1 \exp(-t/\lambda) + \delta_2 \qquad (8)$$

Relaxation times were fit to a linear temperature form, from which predicted values at 131.6°C and 129.2°C were found to be 97 s and 105 s, respectively.

The relaxation behavior following step-shear strains ranging from 20% to 100% was monitored at several temperatures ranging from 141°C to 200°C. Similar to the four-roll mill experiments, the initial 10 s were eliminated, and the results were again fit to a single relaxation time using eq. (8). The relaxation time at 141°C was found to be 52.3 s, which compares well with the value of 50 s obtained from the droplet deformation experiment at the same temperature.

Flow-Induced Crystallization

Figure 7 shows simultaneously recorded birefringence and dichroism video images for a typical flow cessation experiment, in this case at 131.6°C.

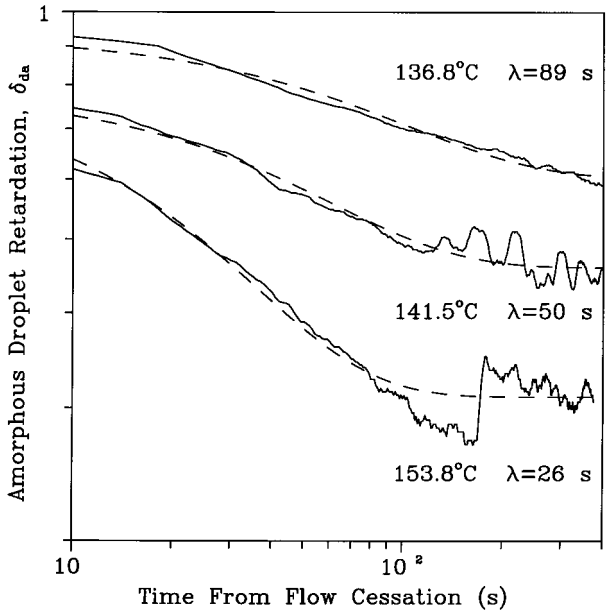

Figure 6 Retardation at the center of the amorphous droplet following cessation of a planar extensional flow at the temperatures indicated. Relaxation times were obtained from best fits of eq. (8), indicated by the dotted lines.

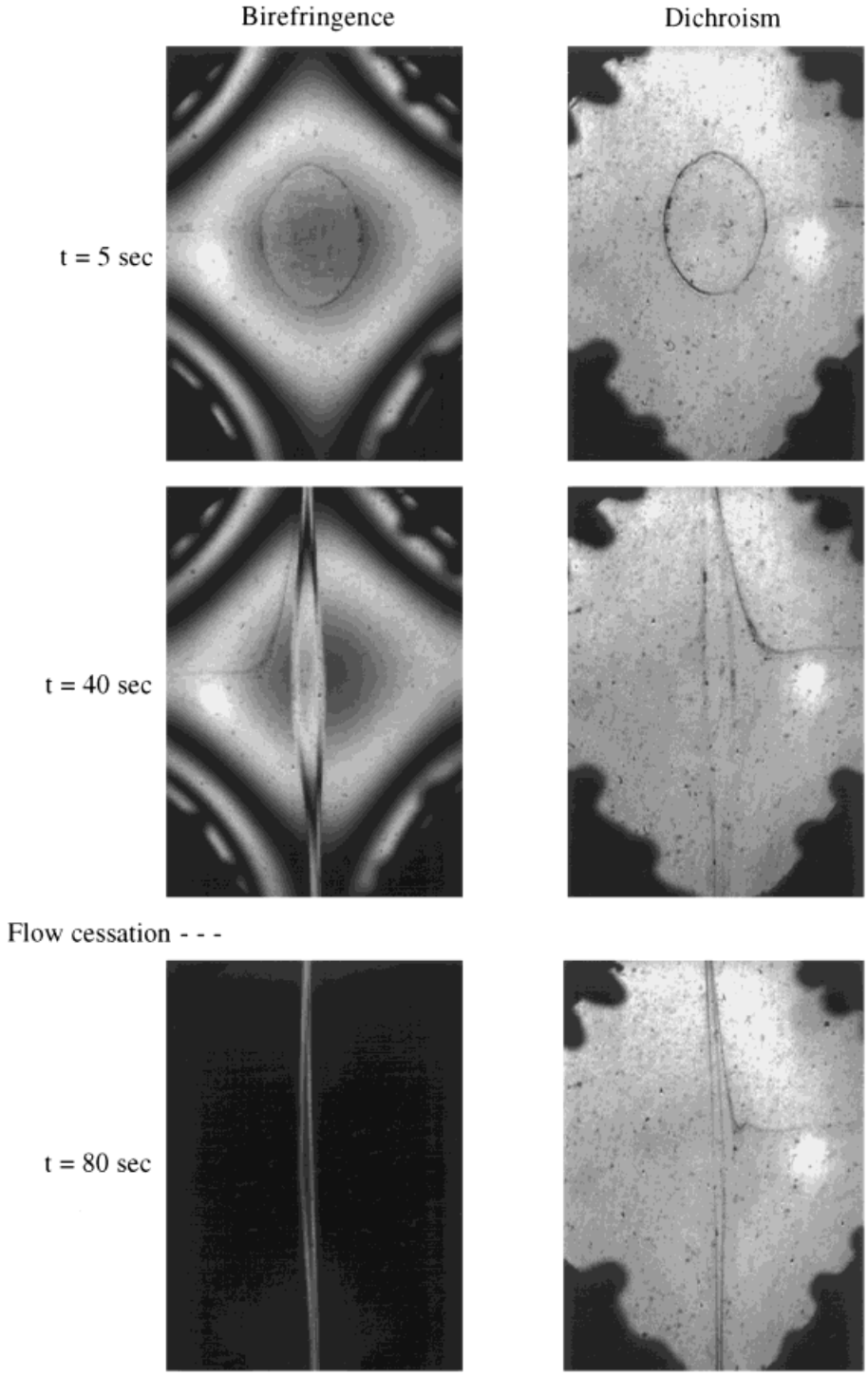

Figure 7 Birefringence (left) and dichroism (right) video images for a flow cessation experiment at 131.6°C. Flow occurred for 1 min at a droplet planar deformation rate of 0.03 s^{-1}.

The flow duration time was 1 min, during which the planar deformation rate in the droplet phase, $\dot{\varepsilon}$ (determined as noted below), was 0.03 s^{-1}. The lack of significant darkening of the dichroism image during flow indicates the absence of crystallization. The difference in isochromatic band separation in

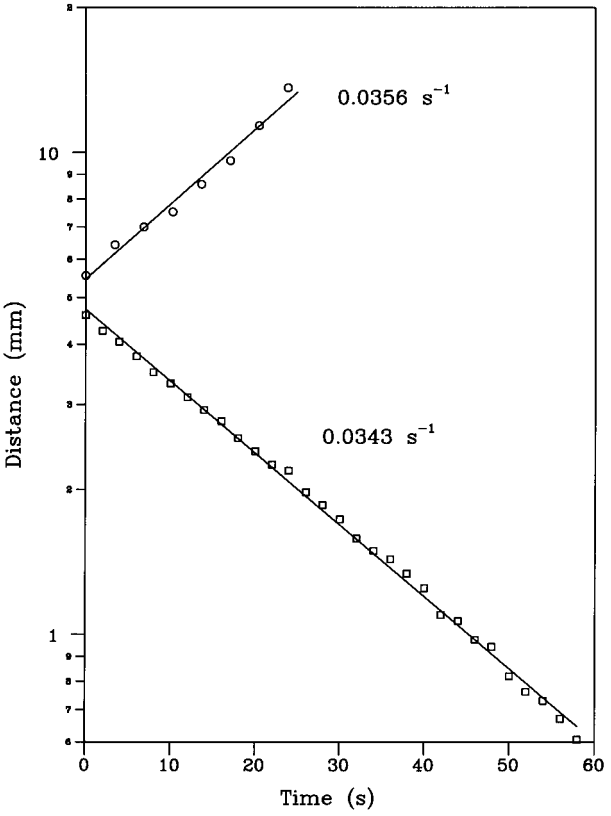

Figure 8 Time dependence of droplet length along the x_1 axis (○) and width along the x_2 axis (□) during flow at 129.2°C. Solid lines are best fits based on eqs. (9) and (10).

the birefringence patterns of the droplet and carrier phases indicates the difference in optical retardation between them. Droplet deformation is related to the Weber number, which gives the ratio of viscous to surface tension forces. Because the surface tension between the two phases is very small, the deformation is smooth and continuous; hence, large deformations are possible. Investigation of an equal-area argument of the deforming droplet, and observations of the ribbonlike nature in the x_3 direction, confirm the two-dimensionality of the flow.[1,3]

Measurements of the time-dependent change in the droplet length and width are used to determine the planar extension rate. A typical example of data obtained from the digitized images is shown in Figure 8. Solid lines are best fits to the displacement equations for planar kinematics, where

$$\frac{l}{l_o} = \exp(\dot{\varepsilon}t) \tag{9}$$

and

$$\frac{w}{w_o} = \exp(-\dot{\varepsilon}t) \tag{10}$$

In these expressions, l and w are the droplet length and width along the x_1 and x_2 axes, respectively. In all cases, the extension rate determined from the length measurement was found to exceed that based on the width dimension, with typical differences on the order of 4%.[3] As discussed elsewhere,[1,3] this reflects the slight inhomogeneity of the hyperbolic flow kinematics in both phases.

Since the carrier phase relaxation time is much lower than that of the droplet ($\sim$ 10 s versus $\sim$ 50 s), its birefringence intensity rapidly drops to zero on cessation of flow, leaving the image of the oriented droplet phase such as shown in the bottom left panel of Figure 7. After a certain time, darkening occurs at the outer edges of the dichroism image, as shown in the lower right panel of Figure 7, indicating the onset of scattering due to crystallization. The dark edges eventually merge and progressively move inward towards the stagnation point as the transformation proceeds. Figure 9 shows dichroism intensity at three axial positions in the droplet phase for a flow cessation experiment at 129°C. The dashed vertical line represents the point of flow cessation (50 s) and the droplet phase planar extension rate during flow was 0.031 s^{-1}. The intensity is essentially constant during flow, whereas, at the point of flow cessation, it begins to decrease due to the onset of crystallization. The positional dependence of the

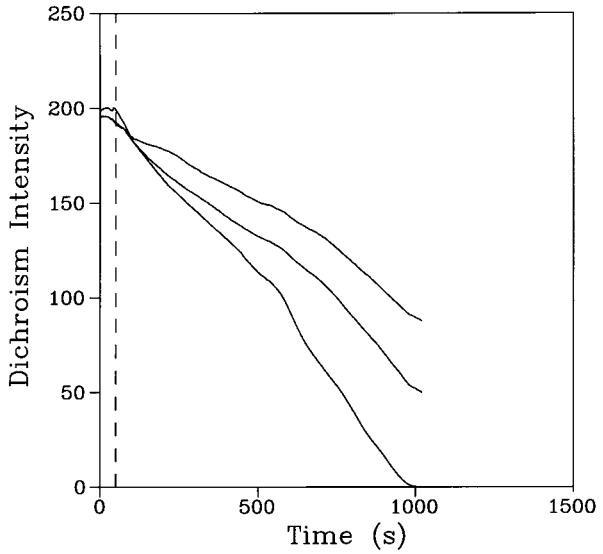

Figure 9 Droplet phase dichroism intensity (arbitrary units) following flow cessation at 129.2°C. Topmost curve is closest to stagnation point; lower curves show increasing axial position from stagnation point. Deformation occurred for 50 s at a planar extension rate = 0.031 s^{-1}.

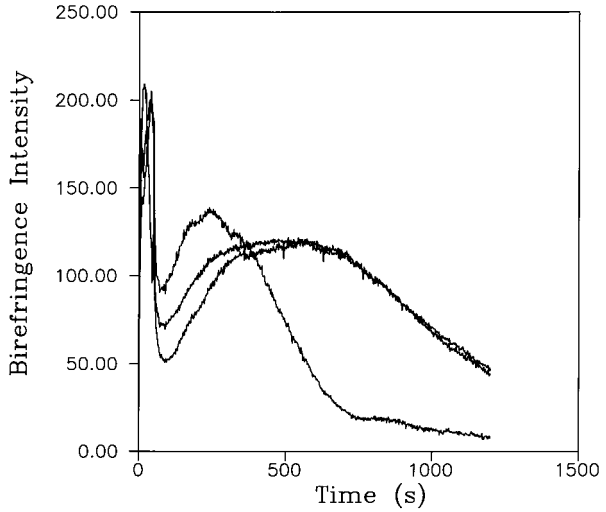

Figure 10 Droplet phase birefringence intensity at the axial positions and conditions of Figure 9. Topmost curve is furthest from the stagnation point.

intensity is consistent with the observation that the dichroism image darkens from the tips inward. This behavior reflects the position dependence of the carrier phase orientation noted earlier[1] and also shows in the slight inhomogeneity of the droplet deformation indicated in Figure 9. Figure 10 shows the birefringence intensity of the same droplet at the axial positions corresponding to Figure 9. The intensity initially drops following flow cessation, and then increases to a fringe maximum during crystallization. Depending on the temperature and flow history, additional fringes may occur.[3] This behavior contrasts with the monotonic drop shown in Figure 6 at higher temperatures, and is another indicator that oriented crystallization is occurring. From Figures 9 and 10 it is clear that flow induces the necessary initial chain extension, which gives way to relaxation and subsequent crystallization following flow cessation. As noted earlier, optical microscopy of extracted samples confirms the c-axis orientation of the crystalline phase.

Continuous Flow Crystallization

Figure 11 shows an example of the time-dependent dichroism intensity measured along optical path A (Fig. 2) for several axial positions in a continuously deforming droplet. In this case, the temperature was 129.2°C and the droplet planar extension rate, $\dot{\varepsilon} = 0.034\ s^{-1}$. The intensity remains essentially constant during a large portion of the deformation until oriented crystallization sets in, at which point there is a rapid drop. Intensity measured along optical path B exhibited a similar time-dependent behavior. In both cases the apparent induction time for crystallization shows a slight decrease as one moves outward from the stagnation point, consistent with the slight inhomogeneity of the flow noted above. In light of this, we limited our observations to the region near the stagnation point where the flow is homogeneous. The quantities κ and, A_e, obtained from eqs. (6) and (7), also exhibit the same time dependence shown by the total intensity. Based on linear fits of these data, both an induction time to crystallization and a rate of crystallization can be determined. In what follows, A_e was chosen as the indicator of crystallinity; however, the same trends result if the phase shift is used.

Figure 12 shows crystallization induction time obtained at 131.6°C for several droplet phase planar extension rates. The data are plotted against the carrier phase birefringence, $\Delta'_{carrier}$. As demonstrated in our earlier study,[1] the latter correlates directly with the molten droplet phase birefringence and therefore gives a measure of the flow orientation in the HDPE phase. The trends shown in Figure 12 suggest a stress–strain rate dependence in the crystallization induction, similar to that found in our earlier flow-cessation measurements.[1]

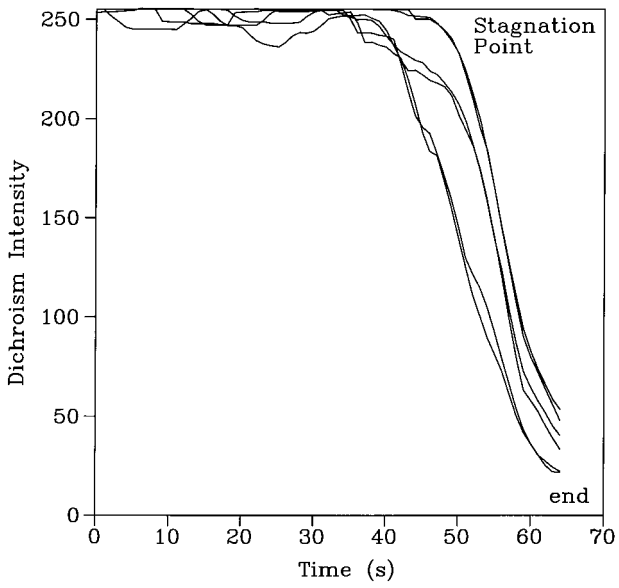

Figure 11 Droplet phase dichroism intensity at various axial positions from the stagnation point versus time at 129.2°C. Droplet planar extension rate, $\dot{\varepsilon} = 0.034\ s^{-1}$.

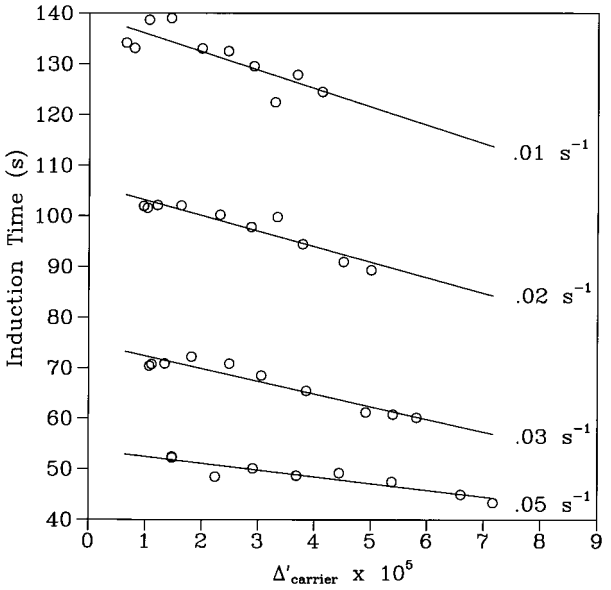

Figure 12 Induction time to crystallization at 131.6°C versus carrier phase birefringence for several indicated droplet deformation rates.

ANALYSIS

Crystallization Model

The competition between molecular relaxation and oriented crystallization is a key feature of FIC which must be accounted for in any model of the process. In a recent article[2] we developed a phenomenological model for FIC which allows this interplay to be quantified. Our approach is based on the Hamiltonian Brackets formalism[6] and incorporates the energetics of stress-induced crystallization and molecular deformation in a manner consistent with the theories of irreversible thermodynamics and continuum mechanics. Flow and stress are described in terms of the elastic dumbbell model which, in the absence of crystallization, leads to the convected Maxwell stress constitutive equation for the fluid. The crystallization component is based on a modification of the model for strain-induced crystallization developed by Gaylord and Lohse[7] which incorporates the effects of uncrystallized portions of the molecule as well as the deformation of the overall amorphous chain in the energetics of the transformation. The resulting equations can be used to model the dynamics of FIC for mixed extension and shear as well as for pure flows. In what follows, parameters evaluated from our rheological and quiescent crystallization data are used in conjunction with the model equations for planar extensional flow to make quantitative comparisons with several of the trends observed in our flow experiments.

The coupled equations for the rate of crystallization, $\partial\phi_c/\partial t$, the normalized molecular conformation tensor, $\bar{\mathbf{c}}$, and the fluid stress tensor, $\bar{\boldsymbol{\sigma}}$, in an isothermal, homogeneous planar extensional flow are the following:

$$\frac{\partial\phi_c}{\partial t} = \frac{\rho}{M_u} Z\Delta H_u\left(1 - \frac{T}{T_m^o}\right) - \frac{nkTZ}{2(1-\phi_c)^2}$$

$$\left(tr\bar{\mathbf{c}} - \left[\frac{24N\bar{c}_{11}}{\pi}\right]^{1/2} + 6N\phi_c - 3N\phi_c^2 + 3\phi_c - 3\right)$$

$$+ \frac{nkTZ}{2}\left[\frac{6\left(1-\frac{4}{\pi}\right)\phi_c N - \left(\frac{24N\bar{c}_{11}}{\pi}\right)^{1/2}}{\bar{c}_{11} + 3\left(1-\frac{4}{\pi}\right)\phi_c^2 N - \phi_c\left(\frac{24N\bar{c}_{11}}{\pi}\right)^{1/2}}\right] \tag{11}$$

$$\frac{\partial\bar{c}_{11}}{\partial t} = 2\dot{\varepsilon}\bar{c}_{11} + \frac{1}{\lambda}$$

$$\times\left[\frac{\bar{c}_{11} - \phi_c\left(\frac{6N\bar{c}_{11}}{\pi}\right)^{1/2}}{\bar{c}_{11} + 3\left(1-\frac{4}{\pi}\right)\phi_c^2 N - \phi_c\left(\frac{24N\bar{c}_{11}}{\pi}\right)^{1/2}}\right]$$

$$- \frac{1}{\lambda(1-\phi_c)}\left[\bar{c}_{11} - \phi_c\left(\frac{6N\bar{c}_{11}}{\pi}\right)^{1/2}\right] \tag{12}$$

$$\frac{\partial\bar{c}_{22}}{\partial t} = -2\dot{\varepsilon}\bar{c}_{22} + \frac{1}{\lambda} - \frac{\bar{c}_{22}}{\lambda(1-\phi_c)}$$

$$\frac{\partial\bar{c}_{33}}{\partial t} = \frac{1}{\lambda} - \frac{\bar{c}_{33}}{\lambda(1-\phi_c)}$$

$$\bar{\sigma}_{11} = -\left[\frac{\bar{c}_{11} - \phi_c\left(\frac{6N\bar{c}_{11}}{\pi}\right)^{1/2}}{\bar{c}_{11} + 3\left(1-\frac{4}{\pi}\right)\phi_c^2 N - \phi_c\left(\frac{24N\bar{c}_{11}}{\pi}\right)^{1/2}}\right]$$

$$+ \frac{1}{(1-\phi_c)}\left[\bar{c}_{11} - \phi_c\left(\frac{6N\bar{c}_{11}}{\pi}\right)^{1/2}\right]$$

$$\bar{\sigma}_{22} = -1 + \frac{\bar{c}_{22}}{(1-\phi_c)}$$

$$\bar{\sigma}_{33} = -1 + \frac{\bar{c}_{33}}{(1-\phi_c)} \tag{13}$$

The normalized conformation tensor, $\bar{\mathbf{c}} = 3\langle \mathbf{R}_N \mathbf{R}_N \rangle / Nb^2$, where $\langle \mathbf{R}_N \mathbf{R}_N \rangle$ is the dyad product of the end-to-end vector of the entire chain, averaged over the configurational distribution function for the elastic dumbbell; and N is the number of statistically-independent links of length b between entanglement points. The stress tensor for the fluid continuum is nondimensionalized with respect to nkT, where n is the number density of molecules, k is Boltzmann's constant, and T is temperature; ϕ_c is the volume fraction crystallinity, ρ is the fluid density, Z is the crystallization rate parameter, M_u is the molecular weight of a chain unit, ΔH_u is the enthalpy of crystallization, and T_m^o is the equilibrium melting temperature of the perfect crystal. In addition, one also has the equation of motion for the incompressible, isothermal, viscoelastic fluid

$$\rho \frac{\partial \mathbf{v}}{\partial t} = -\rho \cdot \nabla \mathbf{v} - \nabla P + \nabla \cdot \boldsymbol{\sigma} \tag{14}$$

where $\mathbf{v}$ is the velocity field and P is the isotropic pressure.

The temperature-dependent crystallization parameter, Z, is evaluated by fitting calorimetric data for the initial rate of crystallization to the simplified form of eq. (11) corresponding to the initial stages of the quiescent transformation

$$\frac{d\phi_c}{dt} = \frac{\rho}{M_u} Z \Delta H_u \left(1 - \frac{T}{T_m^o}\right) \tag{15}$$

Figure 13 shows the resulting Z values fit to an exponential temperature form. Based on the rheological experiments described earlier, a value of 50 s is appropriate for the relaxation time, λ. The number of statistical segments between entanglement points, N, can be obtained from the entanglement molecular weight of the droplet phase material, evaluated in terms of the plateau modulus, G_N^o:

$$M_e = \frac{\rho RT}{G_N^o} \tag{16}$$

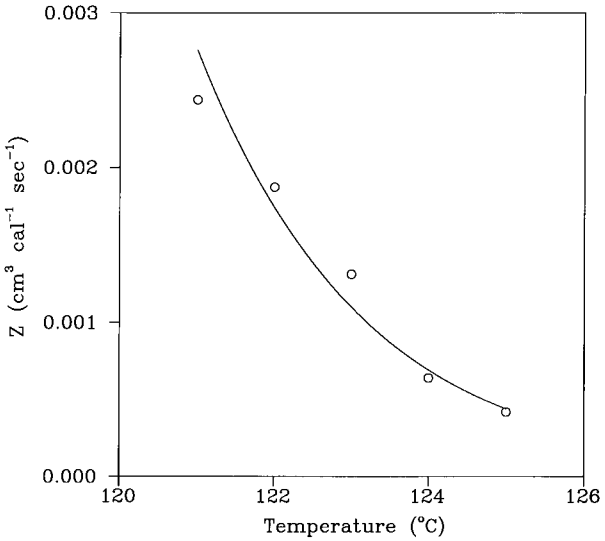

Figure 13 Temperature dependence of the quiescent rate parameter determined from calorimetric data for the HDPE droplet phase material.

G_N^o can be obtained from either the storage modulus or step-strain relaxation data discussed earlier. From our data we obtained a value of 150,000 g mol^{-1}; hence, in the model calculations, we set N equal to 10,000. For polyethylene at low degrees of crystallinity, the total birefringence of the semicrystalline state, Δ_T', can be calculated from the following expression:

$$\Delta_T' = f_c \phi_c \Delta_c + C(\sigma_{11}^* - \sigma_{22}^*)(1 - \phi_c) \tag{17}$$

where f_c is the Hermans orientation factor, which gives a measure of the crystallite orientation relative to the x_1 axis; Δ_c is the birefringence of the perfectly ordered crystal; C is the stress-optic coefficient for the amorphous phase; and the asterisked stresses refer to the completely amorphous melt. The latter is obtained from eq. (13) with $\phi_c = 0$. Although eq. (17) assumes uniaxial crystallite orientation, it has been shown to hold for biaxially oriented polyethylene as well.[8] In our model, f_c must either be estimated or used as a free parameter to fit experimental data. Since our objective was to compare model calculations with data trends, we used the former approach. Values of f_c in the literature[9] are typically on the order of 0.2 for fiber spinline experiments in which stress levels are on the order of 1×10^7 dyne/cm^2. Since stress levels in our system are two orders of magnitude lower, a value of 0.02 for f_c can be considered a reasonable estimate.

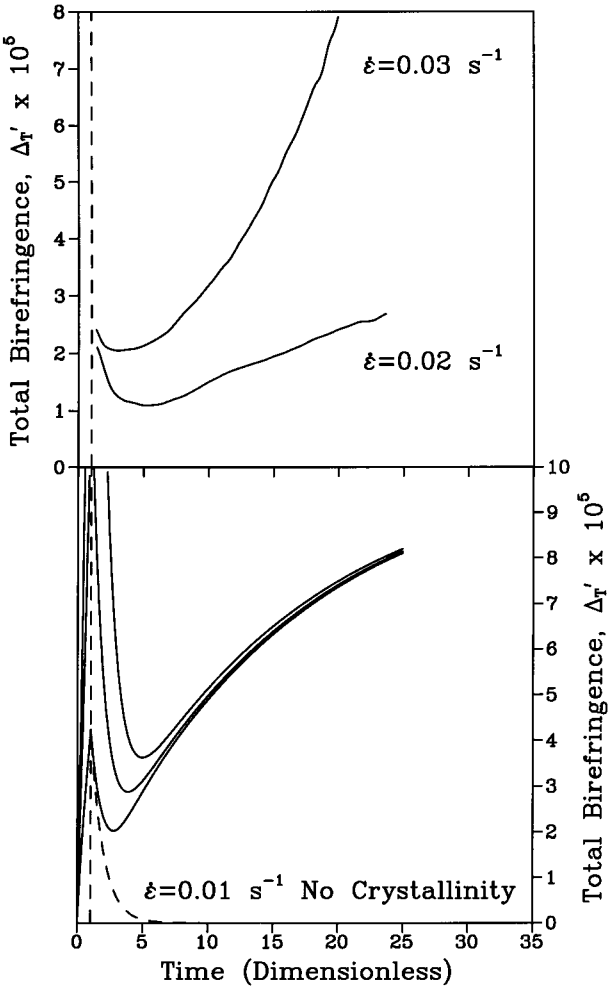

Figure 14 Measured (top panel) and calculated (lower panel) total birefringence following flow cessation at 131.6°C. Topmost calculated curve is for a deformation rate during flow, $\dot{\varepsilon} = 0.03\ s^{-1}$, middle curve for $\dot{\varepsilon} = 0.02\ s^{-1}$, and bottommost curve is for $\dot{\varepsilon} = 0.01\ s^{-1}$. In both the experiment and the calculations, flow occurred for one dimensionless time unit. Dotted curve in lower panel shows predicted behavior in the absence of crystallization for $\dot{\varepsilon} = 0.01\ s^{-1}$.

The discussion which follows is limited to the flow-cessation experiments.

DISCUSSION

A sample comparison of the measured and calculated total birefringence behavior following flow cessation is shown in Figure 14. The experimental data in the top plot are an average for several runs made at the indicated planar extension rates and are typical of the behavior observed in this and the earlier study.[1] Relaxation of the deformed chains following flow cessation causes an initial decay in the birefringence which is subsequently counteracted by the orienting effects of the crystallization. The bottom plots illustrate that the same qualitative trends and quantitative magnitudes are predicted by the model. The dotted line in the bottom panel illustrates the monotonic decay that would occur in the absence of crystallization. The distinct separation in the minima with increased extension rate is common to both plots. The predicted total birefringence at long times is almost entirely due to the oriented crystallization because the amorphous portions of the chains have completely relaxed. It is for this reason that the theoretical curves tend to converge. As noted, eq. (17) is strictly true only for the initial period of the crystallization. A more accurate model which incorporates the effects of increased stress on the amorphous chains due to the increased crystallinity might correct for the lack of separation of the total birefringence curves at long times.

An example of the predicted time dependence of the crystallization following flow cessation is illustrated in Figure 15 for various strain rates during the flow period at 129.2°C. Initial slopes of these curves yield a single value of the crystallization rate for the Hencky flow strain (i.e., $\dot{\varepsilon}t$, where t is the deformation time) when plotted as a function of the melt flow birefringence.[3] Al-

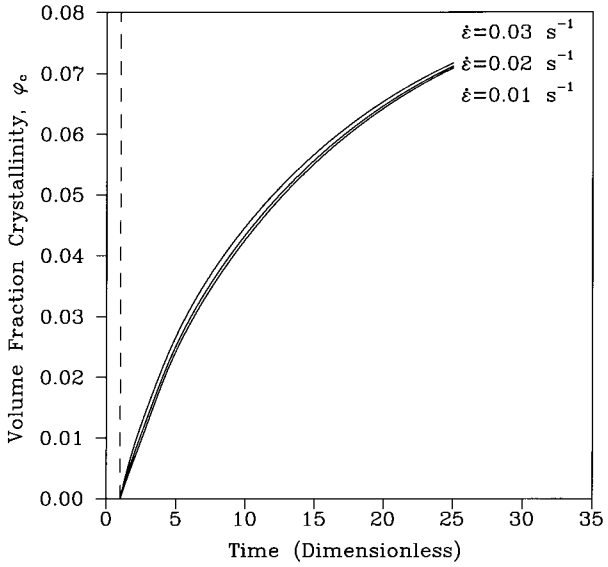

Figure 15 Predicted volume fraction crystallinity following flow cessation at 129.2°C. Flow occurred at the indicated planar deformation rates up to the dimensionless time indicated by dashed line.

though the increase in crystallization rate with strain rate and deformation time is consistent with our experimental trends, a family of points is actually observed experimentally for each Hencky strain.[1] This stress–strain dependence in the initial crystallization rate is a characteristic which, to our knowledge, is not predicted by any of the FIC models.

CONCLUSIONS

The results and discussion presented in this paper illustrate that molecular relaxation plays an important role in the dynamics of FIC. *In situ* measurements of birefringence and dichroism show the evolution of crystallinity as it occurs during continuous extensional flow or during the relaxation period following flow cessation. In both cases, time-dependent molecular orientation results from a competition between relaxation and crystallization processes. Model calculations illustrate this interaction and provide a basis for interpreting experimental data trends.

This work has been supported in part under a grant from the National Science Foundation (grant DMR 89-20538), administered through the Materials Research Laboratory at the University of Illinois.

REFERENCES

1. A. J. McHugh, R. K. Guy, and D. A. Tree, *Colloid Polym. Sci.,* **271,** 629 (1993).
2. A. C. Bushman and A. J. McHugh, *J. Polym. Sci., Part B: Polym. Phys., Ed.,* **34,** 2393 (1996).
3. A. C. Bushman, Ph.D. dissertation, University of Illinois, 1995.
4. A. C. Bushman, master's thesis, University of Illinois, 1993.
5. M. H. Wagner and A. Demarmels, *J. Rheol.,* **34,** 943 (1990).
6. A. N. Beris and B. J. Edwards, *Thermodynamics of Flowing Systems,* Oxford Press, New York, 1994.
7. R. J. Gaylord and D. J. Lohse, *Polym. Eng. Sci.,* **16,** 163 (1976).
8. A. J. McHugh, in *Rheo-Physics of Multiphase Polymeric Systems,* J. Lyngaae-Jørgensen and K. Søndergaard, Eds., Technomic Publishing Co., Inc., Lancaster, PA, 1995, p. 227.
9. J. L. White and M. Cakmak, *Adv. Polym. Tech.,* **6,** 295 (1986).